ACKNOWLEDGMENTS

We would like to thank our supervisor, Pr. Aliseda, for his help during all our researches, his precious advice and his trust in our project.

We also want to express our deep gratitude to our tutor, Dr. Javaherchi, for his kindness, his availability, his patience and his support during and after work. He gave us a lot of his own time and we are very thankful to him.

We want to give special thanks to all the students of the laboratory, who have made us feel welcome.

We finally would like to thank CC Bachelier for his trust in our project.

Numerical Investigation of laboatory-scale horizontal axis marine turbine arrays.

Students : EV2 Moreau, EV2 Percie du Sert, EN2012

Laboratory : Department of Mechanical Engineering, UNIVERSITY OF WASHINGTON

Director of research : Professor Alberto Aliseda

Project tutor : Doctor Teymour Javaherchi

Officer in charge : CC Bachelier

RESUMÉ:

Les turbines marée-motrices sont une source d'énergie renouvelable récente et prometteuse. Pour pouvoir les exploiter au mieux sur des espaces restreints, des études préalables sont nécessaires. La modélisation informatique permet de s'affranchir du coût et du temps nécessaires à une étude expérimentale. L'objectif de ce projet est d'approfondir les connaissances sur l'efficacité de différents réseaux de turbines, à l'aide du logiciel Fluent. Nous nous sommes tout d'abord concentrés sur une appproche macroscopique et rapide d'un premier réseau, qui nous a permis de compléter les données issues de précédents travaux. Nous nous sommes ensuite penchés sur un étude plus fine d'un autre réseau, pour laquelle les modèles de turbulence actuels ne sont pas assez précis et ont besoin d'être modifiés pour correspondre à la réalité.

ABSTRACT:

Marine Hydrokinetic Turbines are a new and attractive source of renewable energy, but to implement them on small areas, scientific and engineering studies have to be conducted. Time and cost of an experimental study can be reduced by using computational fluid dynamics simulations. The goal of this project is to investigate on the efficiency of different turbines arrays, using a commercial software package for CFD simulations (Fluent, Ansys Inc. Cannonsburgh, PA). We first focused on an overall study of a first array, and we compared against experimental data from a previous study. We then tackled the issue of a high-fidelity analysis of another array configuration, but the turbulence models available for this simulation were not accurate enough for a successful comparison. Further research on the topic of turbulence closure models for rotating systems, in which the free-stream turbulence is elevated, as it happens in marine currents where it is routinely measured at over 5%-10%, is recommended as necessary for accurate prediction of the wake recovery in turbine arrays.

About the Multiphase & Cardiovascular Flow Lab, in the Department of Mechanical Engineering.

The Cardiovascular and Multiphase Flows Lab works on fundamental problems in fluid mechanics that arise in turbulent and complex, unsteady flows, in many cases with the addition of a second disperse phase. Turbulence is one of the last answered question in classical physics. When more than one phase is present, such as when liquid droplets are injected into a gas stream, or when air bubbles are introduced into a water flow, new and interesting phenomena occur that are both scientifically challenging and relevant to many engineering and environmental applications. Their approach is to perform experiments, complemented with numerical simulations and theoretical analysis, in order to probe the fundamental physical processes involved. Once the key features of the problem are understood, they develop a quantitative model that can be incorporated into large scale, multiphysics models for applications.

Examples of fluid mechanics problems that they are addressing are the dynamics of water droplets or solid spherical particles in a turbulent air flow; the hydrodynamics of microbubbles in non-uniform flows; the breakup, transport and impact of liquid droplets made up of complex fluids; the influence of fluid and solid mechanics on the origin and progression of cardiovascular disease on the carotid bifurcation and on arterio-venous fistulas for dialysis access. They are also involved in the study of tidal and in-stream turbines for renewable energy generation from marine currents. This project is part of the National Northwest Marine Renewable Energy Center created in the Fall of 2008 by the US Department of Energy to advance marine renewable energy conversion in the US. Their interest is in modeling, numerically and experimentally, the flow around turbine blades and the resulting wake, with a particular emphasis on wake turbine interactions and short range environmental effects, such as pressure fluctuations and sediment transport [1].

TABLE OF CONTENTS

Page

List of Figures . . . 3

Chapter 1: Introduction . . . 1
1.1 Introduction to Renewable Energy Research . . . 1
1.2 Tides and currents . . . 1
1.3 Literature review . . . 3

Chapter 2: Numerical methodology . . . 5
2.1 Navier-Stokes equations . . . 5
2.2 Reynolds-Averaged Navier-Stokes equation . . . 6
2.3 Turbulence models . . . 7
The k-ε model. . . . 7
The k-ω model. . . . 8
The SST k-ω model. . . . 8
2.4 The Single Reference Frame (SRF) . . . 8
2.4.1 Theory . . . 8
Purpose of this numerical model. . . . 8
Theory of the SRF. . . . 9
Specific boundary conditions. . . . 10
2.4.2 The meshing process . . . 11
Difficulties in the process. . . . 11
Arguments to create only one nacelle. . . . 14
2.5 Blade Element Model (BEM) . . . 15
2.5.1 Theory . . . 15
2.5.2 The meshing process . . . 16

Chapter 3: BEM Simulations of an Array of Three Turbines with 0.25D Lateral Offset and Downstream Spacing of 5D and 7D . . . 19
3.1 Simulation of Experimental Setup and Condition . . . 19

3.2 Results for a three-turbine array with 5D downstream spacing 20
Region of low TSRs (<7) 23
Region the optimum TSR. 24
Region of high TSRs. 25
3.3 Differences between 5D and 7D spacing 25
3.4 Blockage effect 25
Blockage creates a gain of efficiency. 26
Blockage shifts the peak of efficiency. 26
The Compound Effect of Blockage, Wake and Shear Flow on the Efficiency of the two Downstream turbines. 30

Chapter 4: The SRF study 31
4.1 MHK Turbine Array Simulations using Single Reference Frame (SRF) Model 31
4.1.1 Efficiency Formulation in SRF Model 31
Chronological Steps of the Investigation 32
4.2 Investigation on the Issue of the SST k-ω Model in Modeling the Far Wake Region 35
4.2.1 Location of the problem 35
4.2.2 Investigation on the model equations 36
4.2.3 Results from simulations with the modified equations 37
4.2.4 Summary and Conclusions 40

Chapter 5: Conclusions and Future work 42
5.1 Array of three turbines 42
5.2 Array of two coaxial turbines 43

LIST OF FIGURES

Figure Number — Page

1.1 Neap and spring tides formation . . . 3

2.1 Front view of a computational domain with a turbine blade inside. (A) the turbine blade is rotating with respect to the stationary frame (unsteady flow field). (B) the blade is stationary and the frame is rotating with respect to the blade (steady flow field) . . . 9

2.2 Top vision of the mesh around the blade. . . . 12

2.3 Top view of the domain to be meshed. . . . 13

2.4 View of the geometry created to mesh the transition region. 13

2.5 View of the final SRF meshed domain. . . . 15

2.6 Computational domain and boundary conditions used with BEM. The effect of the turbine is modeled via body forces applied on the disk swept by the rotor (gray region). . . . 16

2.7 Three turbines separated by 5 rotor diameters in the streamwise direction and 0.25 rotor diameters in the transverse direction, meshed on GAMBIT. . . . 17

3.1 Normalized streamwise velocity contours by the freestream velocity at the inlet for TSR=7.16 . . . 21

3.2 Numerical versus experimental results for arrays of three turbines with 0.25D lateral offset 5D downstream spacing operating under various TSRs. . . . 21

3.3 Normalized kinetic energy flux and Turbulent kinetic energy in front of each turbine for a TSR=8 . . . 22

3.4 Rotational speed normalized by mean rotational speed over one minute for a high TSR operating condition and a low TSR operating condition. . . . 24

3.5 Numerical results for arrays of three 0.25D lateral offset turbines with 7D downstream spacing, versus 5D spacing, at different TSR. . . . 26

3.6 Numerical results for arrays of three turbines at 0.25D lateral offset and 5D downstream spacing, simulated at various blockage ratios. 27
3.7 Qualitative explanation of the shift of efficiency due to blockage for a single turbine operating under various TSR. 28
3.8 Lift coefficient as a function of Angle of Attack for a NACA4415 profile (Points are placed qualitatively). 29
4.1 Comparison of measured and predicted variation of the velocity deficit at various distances downstream of the first turbine, with TSR=7.16. 34
4.2 Comparison of turbulent intensity between the standard SST k-ω model and the modified SST k-ω model. 38
4.3 Comparison of measured and predicted variation of the velocity deficit at various distances downstream of the first turbine, with TSR=7.16, using the modified SST k-ω model 39

Chapter 1

INTRODUCTION

1.1 Introduction to Renewable Energy Research

The planet is facing big challenges : global warming, pollution and the need to manage diminishing fossil fuel reserves. To protect the generations to follow, it is commonly accepted that we have to reduce our emission of greenhouse gasses. That is why, in 1995, most countries in the international community ratified the Kyoto Protocol. They had, between 2008 and 2012, to reduce by 5% their 1990 greenhouse gasses emission. So the concept of supporting renewable energy sources as a matter of national policy to reduce fossil fuel relative weight in energy generation was introduced.

Renewable energy refers to an energy resource that will be naturally and quickly regenerated [2]. It can come directly from the sun (such as thermal, photochemical or photoelectric), indirectly derive from the sun (such as wind) or come from other natural movements and mechanisms of the environment (such as tides). In this project, we will focus on this type of energy. Indeed, tidal energy is beginning to be developed. There are strong similarities to wind energy but important differences such as influence of free surface, stratification, strong confinement in constricted channels, etc.) still need to studied to determine its economic viability (cost of energy, efficiency, ...) as well as its environmental footprint (sediment transport, impact on the wildlife, etc.).

1.2 Tides and currents

According to Newton's law of gravitation, two bodies attract each other with a force that is proportional to the product of their mass and inversely proportional to the

square of the distance between them. Moreover, the attraction force points along the line intersecting the centers of mass. Thus, the gravitational force between two bodies, of masses m_1 and m_2, and with a distance r between them, will be :

$$F = G \times \frac{m_1 m_2}{r^3} \tag{1.1}$$

where G is the universal gravitational constant and is equal to $6.67384 \times 10^{-}11 m^3 \cdot kg^{-1} \cdot s^{-2}$. This force is responsible of tides. Indeed, sun and moon attract the earth and the water on its surface. As the position of sun and moon changes, the oceans flow in response to that attraction. Moreover, because it is closer to Earth than the sun, the moon is responsible for 70% of tides.

Spring and neap tides are, respectively, the higher and the lower sea levels. As shown on figure 1.1 (source : Engineering Department of Lancaster University website) , spring tide is reached when moon, sun and earth are all on the same axis. Therefore, the effects of the two gravitational forces are added together. Neap tide, on the other hand, is reached when the moon-earth axis is perpendicular to the sun-earth because the forces induce flows in opposing directions.

These variations in the sea level generate strong currents in places where the water is forced to flow through a narrow passage. Because the flux of kinetic energy is proportional to the cube of the flow velocity, MHK turbines are particularly effective and therefore will be economically viable, in those regions.

$$P = \frac{1}{2}\rho S V^3 \tag{1.2}$$

where ρ is the density of the water, S is the cross-sectional area of the water passage and V is the average velocity of the flow. P, the flux of kinetic energy, is also proportional to the area that the current goes through but the velocity term is prevalent in the equation thanks to the cube. So, because the flow accelerates in narrow passages, the available flux of kinetic energy will be more significant in this type of places.

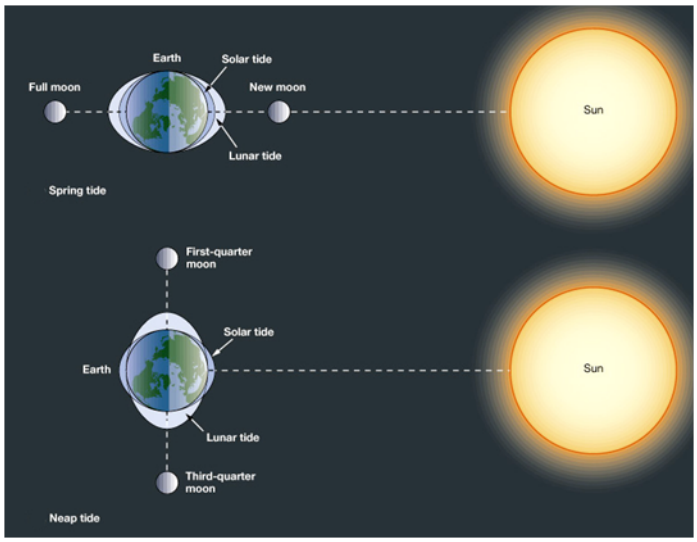

Figure 1.1: **Neap and spring tides formation**

Even if tidal energy seems to have a lot of similarities with wind energy, there is some advantages in using Marine Hydrokinetic (MHK) turbines :

- tidal energy is more consistent because currents alternate but never stop whereas wind does.
- currents are more easily predictable than wind.
- even if the velocity of tides is smaller than the wind one, the density of the sea water, which is 850 times bigger than air, makes the available energy flux (P) similar or even a little stronger for MHK turbines than for wind turbines.

1.3 Literature review

Before being able to extract energy from tidal currents, it has to be researched to be certain this energy will be effective and efficient. But building and experimenting on a real-scale array of turbines is not feasible, for the price and the time of such a

study. That is the reason why we need reliable numerical models. Indeed, numerical simulations are less expensive than experiments. So one methodology is building lab-scale experimental models and running experiments on them. Then, once the lab-scale numerical model is created, it is possible to run simulations and see if the results are matching the experiment. If they do, then it is viable to run numerical simulations to optimize designs and understand the limitations in operating conditions. Simulations can then be conducted for a few selected cases on full-scale models. Finally, once the full-scales simulations have yielded understanding of the conditions and performance of the optimized designs, the last step is to build a full scale turbine prototype to confirm the results from the lab-scale simulations and experiments and the full-scale simulations.

N. Stelzenmuller, in his Masters thesis [3], conducted experiments on lab-scale Horizontal Axis Hydrokinetic Turbines (HAHTs). He collected measurements on a single turbine, on arrays of three turbines placed coaxially, and on arrays of three turbines placed with a lateral offset. In his PhD thesis, [4], T. Javaherchi created different numerical models for a single turbine and for arrays of coaxial turbines, with good agreement of the computational results with the experiments of N. Stelzenmuller. Arrays of two coaxial turbines with a high-fidelity model, and of three turbines with a lateral offset were, however, not studied.

In this work, we based our simulations on T. Javaherchi's work, extending them to new conditions that had been measured experimentally but not modeled computationally before. Our first step has been to work on the arrays described in the previous paragraph, and validate our results against experiments. After that, when we were sure that the numerical results were reliable, they were exploited to determine the advantages and drawbacks of each array.

Finally, we focused on the flow field and the performance analysis of MHK turbines in an array of two coaxial turbines, with a more precise model, and compared them against N. Stelzenmuller experimental data.

Chapter 2

NUMERICAL METHODOLOGY

2.1 Navier-Stokes equations

The Navier-Stokes equation describes the motion of a fluid in an Eulerian reference frame. This equation comes from the Newton's second law of dynamics, and represents the conservation of momentum in the fluid flow. The equations can be simplified to obtain a form that is commonly used in many engineering and environmental fluid mechanics problems: assuming a Newtonian fluid, fluid density ρ is constant, dynamic viscosity μ is also constant, and the fluid is incompressible, the resulting equation is:

$$\rho\frac{\partial}{\partial t}\vec{v} + \rho\vec{v}.\nabla\vec{v} = \mu\Delta\vec{v} - \nabla p + \vec{f} \tag{2.1}$$

where $\vec{v}$ is the velocity of the fluid and p the pressure. The physical meaning of the different terms are as follows:

- $\rho\frac{\partial}{\partial t}\vec{v}$ is the unsteady acceleration
- $\rho\vec{v}.\nabla\vec{v}$ is the convective acceleration
- $\mu\Delta\vec{v}$ represents the viscous forces
- ∇p is the pressure gradient
- $\vec{f}$ are the external body forces

A dimensionless quantity is introduced by this equation, the Reynolds number, which is defined as the ratio of inertial forces to viscous forces.

$$R_e = \frac{\rho V_\infty L}{\mu} \tag{2.2}$$

This number is used to define the flow regime, either laminar (low R_e) where viscous forces are dominant, or turbulent (high R_e) where inertial forces are dominant and the non-linear convective term results in a chaotic state of motion that can only be described in a statistical sense. In our case, with a fluid density of 998.2 $kg.m^{-3}$, a velocity of the order of 1 m/s, and a length scale of the order of 10 m, the Reynolds number is around 10^7, we are in a turbulent regime.

2.2 Reynolds-Averaged Navier-Stokes equation

This section was written based on [5] and [6].

When using Computational Fluid Dynamics (CFD), we want to solve the Navier-Stokes equation. A turbulent flow instantaneous solve this equation. But it is impossible to predict the flow in detail, that is to find a deterministic solution to the velocity and pressure in the flow at each location and at each time. To solve the equations computationally, solving each scale of the motion would require an enormous time (Direct Numerical Simulation or DNS). Fortunately, we are more often interested in finding only the average characteristics in such a flow, so we can simplify this equation. The method used here is called the Reynolds decomposition, for we are decomposing the flow variables into their mean part and a deviation from the mean;

$$v = \overline{v} + v' \tag{2.3}$$

$$p = \overline{p} + p' \tag{2.4}$$

By projecting the Navier-Stokes equation along the vector $\vec{i}$ of a reference frame, we obtain a new formulation of Eq (2.1);

$$\rho\frac{\partial v_i}{\partial t} + \rho v_j \frac{\partial v_i}{\partial x_j} = \mu\frac{\partial^2 v_i}{\partial x_j^2} - \frac{\partial p}{\partial x_i} + f_i \tag{2.5}$$

When substituting Eq (2.3) and Eq (2.4) in this equation, and averaging it, we obtain the Reynolds averaged Navier-Stokes equation (RANSE);

$$\rho\frac{\partial\overline{v_i}}{\partial t}+\rho\overline{v_j}\frac{\partial\overline{v_i}}{\partial x_j}=\mu\frac{\partial^2\overline{v_i}}{\partial x_j^2}-\frac{\partial\overline{p}}{\partial x_i}+f_i-\rho\frac{\partial}{\partial x_j}(\overline{u_j'.u_i'}) \tag{2.6}$$

The last term of this equation, the Reynolds stress tensor, is the effect of the turbulence (fluctuations about the mean) on the evolution of the mean flow. This term adds a number of unknowns to the system, with the number of equations unchanged. To solve Eq (2.6), we need a closure model to match the number of equations and the number of unknowns. We close the system by using a relation of the type:

$$\overline{u_j'.u_i'}=\frac{2}{3}k\delta_{i,j}-\nu_t(\frac{\partial u_i}{\partial x_j}+\frac{\partial u_j}{\partial x_i}) \tag{2.7}$$

where ν_t is the turbulent viscosity and k the turbulent kinetic energy. These variables are given by a turbulence model, so that we will be able to solve the Reynolds-Averaged Navier-Stokes equation (2.6).

2.3 Turbulence models

This section was written based on [7].

In this study, we use 3 different two-equation models that have been developed and tested to simulate turbulent flows, with different features, and compared against experimental measurements, typically in wind-tunnel configurations. We will only briefly describe these models, we shall speak more about one of these models in the SRF study.

The k-ε model. This model is based on a specification of the turbulent viscosity and on two transport equations, one for the kinetic energy (k) and the other one for ε, which stands for the dissipation rate of k. This model is known to be good for free-shear flows, such as the wake after a turbine, but not as good on the near-wall

region. It will be used on the VBM study, where no wall-conditions (no-slip) are imposed on the flow.

The k-ω model. This model uses ω which stands for the turbulence frequency, k and ν_t remain the same as in the previous model. It solves equations linked to the transport of ω and k. The difference with the k-ε model is a different equation used for ω. This model is known to be more accurate on the viscous near-wall regions than the k-ε model.

The SST k-ω model. This model is designed to yield the best behavior of the k-ε and the k-ω models. It is written as a k-ω model with a blending function, which will result in the properties of the k-ω model near the walls and of the k-ε model far from the walls. This model seems to be the best for a global study, since it uses properties of both k-ε an k-ω models, and it will be used for the SRF study.

2.4 The Single Reference Frame (SRF)

2.4.1 Theory

This section was written based on [8] and [9].

Purpose of this numerical model. Many applications on computational fluid dynamics deal with rotating elements on a flow field, therefore they cannot be studied on a stationary reference frame, because the rotating objects (blades, propellers, windmills) render the problem unsteady. The main idea behind the Single Rotating Reference Frame is to render this unsteady problem on a stationary frame into a steady problem on a rotating frame. To achieve this, the reference frame is rotating steadily at the angular velocity of the rotating object (in our study, a blade), along the axis of rotation, according to Figure 2.1 [10].

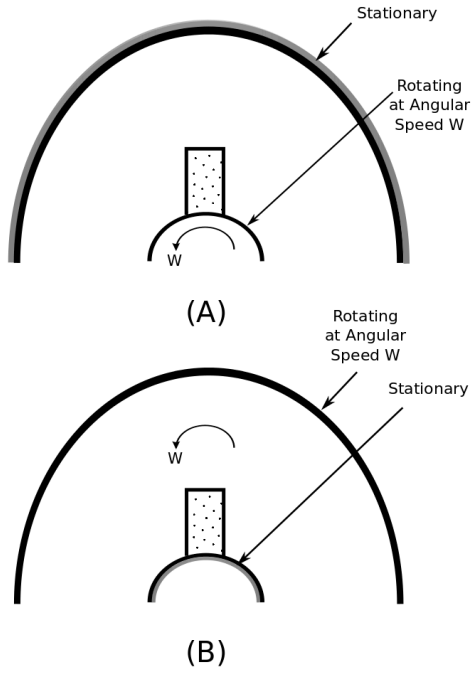

Figure 2.1: **Front view of a computational domain with a turbine blade inside. (A) the turbine blade is rotating with respect to the stationary frame (unsteady flow field). (B) the blade is stationary and the frame is rotating with respect to the blade (steady flow field)**

As the entire domain is studied as one rotating frame, this model is called Single Reference Frame. This is in contrast with other models with rotating objects where the domain is divided into several subdomains, and in these subdomains, different reference frames are used. These models are called Multiple Reference Frame and are used for example in turbo-machinery.

Theory of the SRF. If the velocity relative to the rotating system is defined as $\vec{v_r}$,the angular velocity of the blade (therefore of the rotating frame) as $\vec{\omega}$ and the position vector of each point in the computational domain, from the origin of the

rotating frame as $\vec{r}$, the composition law holds;

$$\vec{v_r} = \vec{v} - \vec{\omega} \times \vec{r} \tag{2.8}$$

with $\vec{v}$ the velocity in the stationary reference frame. The equations of conservation cannot be solved in the rotating reference frame. Since the entrainment velocity does not contribute to the mass balance, the equation of mass conservation remains invariant and can be written as;

$$\frac{\partial \rho}{\partial t} + \rho \nabla \vec{v_r} = 0 \tag{2.9}$$

For the conservation of momentum, two more forces shall be added, since the inertia term $\frac{\partial \vec{u}}{\partial t}$ is not invariant when passing from one reference frame to another. These two forces are the Coriolis force per unit mass ;

$$\vec{f_C} = -2(\vec{\omega} \times \vec{v_r}) \tag{2.10}$$

and the centrifugal force per unit mass;

$$\vec{f_c} = -\vec{\omega} \times (\vec{\omega} \times \vec{r}) \tag{2.11}$$

The addition of these two forces in the Navier-Stokes equation (2.1) leads to the following equation for conservation of momentum;

$$\rho \frac{\partial \vec{v_r}}{\partial t} + \rho \vec{v_r}.\nabla \vec{v_r} + \rho(2\vec{\omega} \times \vec{v_r} + \vec{\omega} \times \vec{\omega} \times \vec{r}) = \mu \Delta \vec{v_r} - \nabla p + \vec{f} \tag{2.12}$$

Specific boundary conditions. With the change of the reference frame, new boundary conditions have to be set, to render this change transparent. The walls that are moving with respect to the stationary reference frame (turbines blades surfaces) are described with a no-slip condition, so that the relative velocity to the rotating reference frame is zero. The walls that are not moving with respect to the stationary reference frame (outer walls of the domain) are described with a slip condition so

that they will not shed any vortices as they move relative to the rotating reference frame. These surfaces need to be also surfaces of revolution about the axis of rotation. The last boundary conditions needed by the SRF model are the rotationally periodic boundaries, which must be periodic about the axis of rotation. Taking advantage of the two-bladed symmetry of the rotor, the domain can be defined with 180 degrees of circumference, instead of using the full 360 degrees circumferential domain. Thus, we can reduce the domain studied without loosing spatial resolution.

2.4.2 The meshing process

In this SRF study, an array of two coaxial MHK turbines will be examined, with a distance of 5 blade diameters between the two turbines. The previous work on such turbines was done by T.Javaherchi [4], who focused on a single turbine. To mesh the two-turbine domain, we had access to the mesh for one single turbine. This mesh was copied and translated 5 diameters downstream. The goal at this point was to connect the end of the first turbine domain with the beginning of the second one.

Difficulties in the process. The major difficulty faced was that the first mesh has been built around the blade, with freedom for both the upstream and the downstream part. As shown on figure 2.2, the blade has a twist and a pitch on its shape, so that the mesh upstream the blade does not match the mesh downstream. The reason behind this difference is that to lower the skewness * without increasing the number of element around the blade, many faces that were twisting around the blade have been divided in several faces, therefore the geometry of the mesh changed and many new mesh edges were created.

---

*According to [11], for equilateral volumes;

$$\text{Skewness} = \frac{\text{Optimal cell size - Cell size}}{\text{Optimal cell size}} \tag{2.13}$$

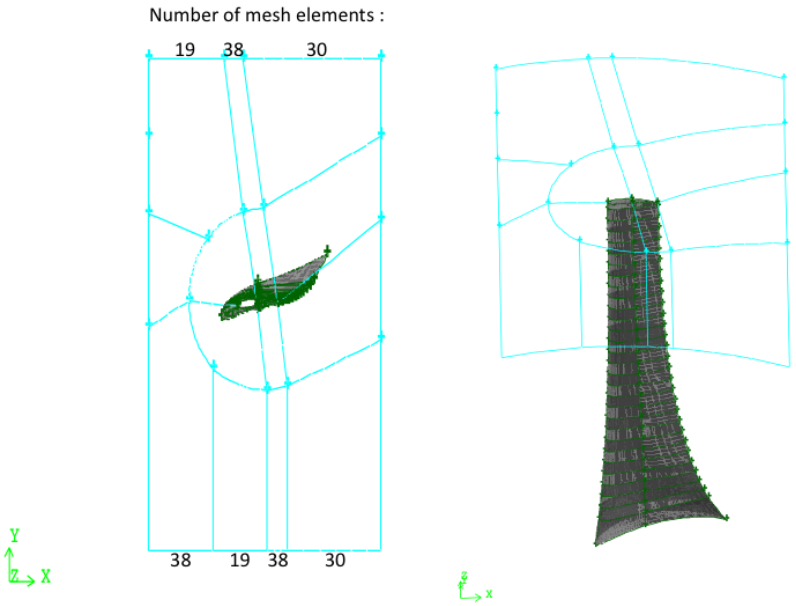

Figure 2.2: **Top vision of the mesh around the blade.**

Therefore, it was not possible to connect the end of the first turbine with the beginning of the second one with only one mesh region, a transition region had to be created. To build this region, the number of mesh elements of the end of the first turbine has to correspond to the number of mesh elements of the beginning of the second turbine, as shown on figure 2.3, while avoiding any high skewed elements. This problem was fixed by creating an original mesh geometry (figure 2.4), and by splitting the structured mesh previously created, so that the the number of mesh elements could match each other, with a good skewness.

Then the second difficulty faced was the nose of the nacelle. On the first mesh, this problem has been avoid by using an algorithm (Cooper) which projects the mesh from the face of a volume on the opposed face. This was possible on the first turbine thanks to the freedom on the upstream part, but was no longer allowed on the second one, which had to match the downstream part of the first turbine. Different scenarios

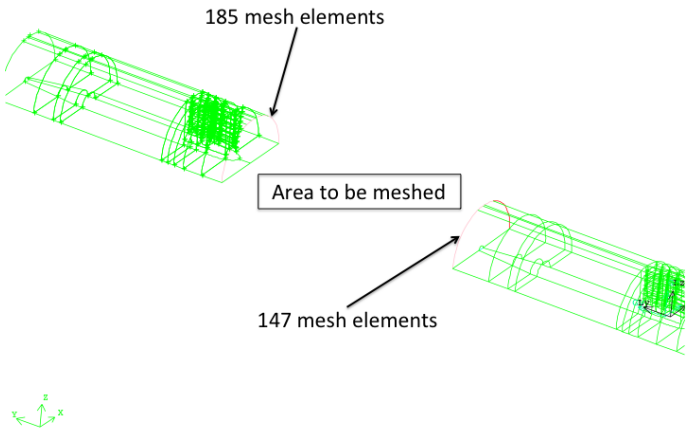

Figure 2.3: **Top view of the domain to be meshed.**

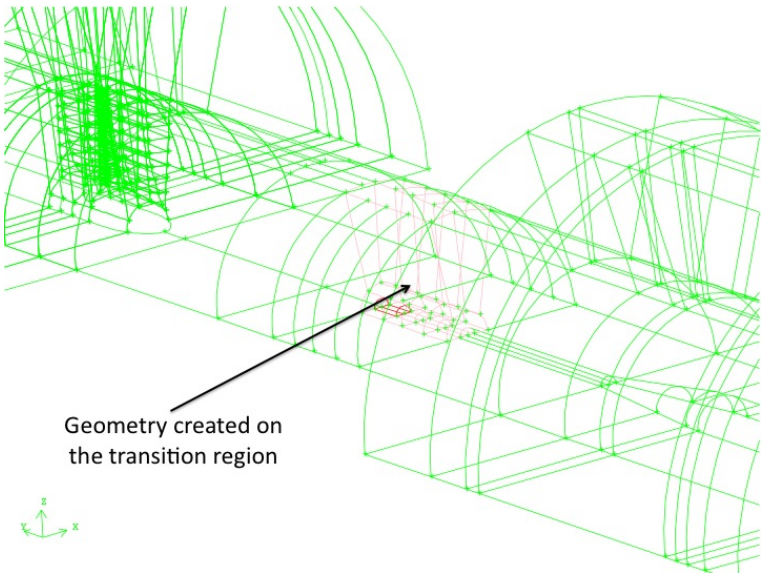

Figure 2.4: **View of the geometry created to mesh the transition region.**

to mesh this part were tried, but the best mesh ended with more than 10 000 high skewed and inverted elements (over 0.85). So the choice was either having a lot of skewed elements on the mesh or remove the source of skewness, i.e the concave part

of the second nacelle nose, and create only one nacelle for the two turbines.

Arguments to create only one nacelle. As discussed earlier creating two distinguished nacelle geometries for two turbines led into an overall low quality mesh with $\approx$ 10000 high skewed and inverted elements. All of the tested solutions to improve the mesh resolution did not result into a significant improvement in mesh quality. Therefore, it was decided to combine the nacelles' geometries of the first and second turbine together. Hence, the computational domain includes one long nacelle for both of the devices (see figure 2.5). Two additional arguments justifying that the combination of the two nacelle geometries would not significantly affect the flow field and performance of the two turbines in the SRF simulations were considered:

- In the SRF simulation, since the flow is rotating around the turbine's axis of rotation if the nacelle's walls was set to a no-slip boundary condition, a set of non-physical vortices would be introduced and contaminate the RANS solution for the flow field (i.e. similar to rotating flow around a cylinder). This is known as an existing limitation in the SRF model. Hence, the actual flow and turbulent boundary layer around nacelle can not be captured precisely in this model. Furthermore, it should be noted that this effect would never be present in the experiment. Indeed in the experiment the flow is parallel to the nacelle and the nacelle geometry leads to a smoother flow direction after power extraction by the turbine blade.

- Merging the two nacelles and excluding a small part between two turbines, which is close to the blades' root would also not affect the performance of the turbines significantly. The reason behind this is that the root's contribution to the performance is minimal and the dominant effect on the efficiency of the blades is coming from the lift produced at the sections close to the blade tip with longer moment arm.

The single nacelle was created and the entire domain was meshed, with 14 352 523 elements and a maximum skewness of 0.91, which came from a few elements on the nose of the first turbine.

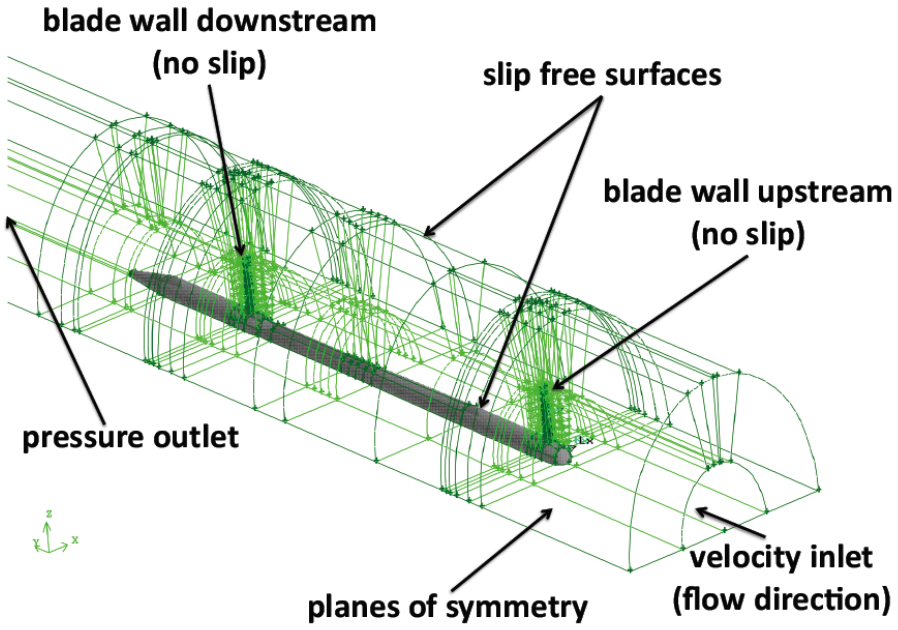

Figure 2.5: **View of the final SRF meshed domain.**

2.5 Blade Element Model (BEM)

2.5.1 Theory

The Blade Element Model is less complex than SRF, therefore easier to setup and less time-consuming. This model is based on the Blade Element Theory [12]. In this theory, the rotating blades of the turbine are modeled by a full disk, much easier to mesh than the whole geometry of the blades. This disk is characterized by several data for different sections along the blade: the chord length, the angle of attack (AOA) and the lift and drag coefficients. For each section from the root to the tip of the blade,

the chord length is provided by the manufacturer and the lift and drag coefficients ($C_{L,D}$) are given in tables depending on the Reynolds number and the AOA.

In the BEM, the effect of the rotating blades is modeled by two body forces applied on the fluid, along rings of the disk we defined previously. These forces have the same absolute value but an opposite sign than lift and drag forces given in Eq (2.14).

$$f_{L,D} = C_{L,D} \cdot c(r/R) \cdot \frac{\rho V_{tot}^2}{2} \tag{2.14}$$

where ρ is the fluid density and V_{tot} is the fluid velocity relative to the blade.

2.5.2 The meshing process

As shown on figure 2.6, the meshing of one single turbine had previously been done by Javaherchi et al.[13].

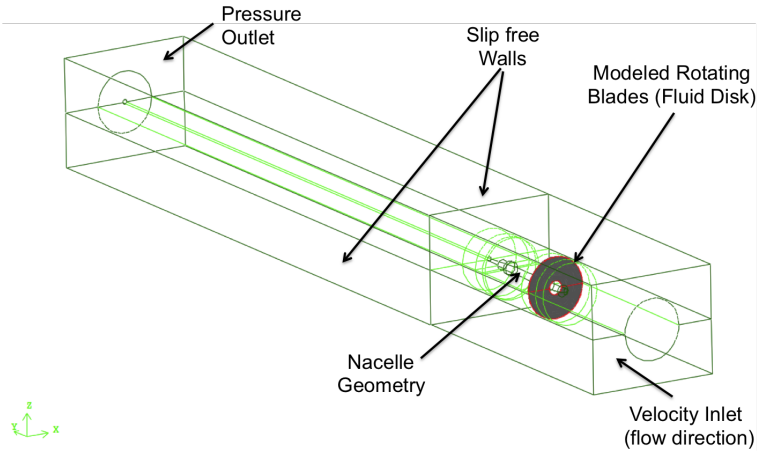

Figure 2.6: **Computational domain and boundary conditions used with BEM. The effect of the turbine is modeled via body forces applied on the disk swept by the rotor (gray region).**

The meshing process began with the mesh of this single turbine. The domain to mesh was an array of three turbines with a 0.25 rotor diameter lateral offset and

a 5 rotor diameter downstream spacing between turbines. The software GAMBIT has been used for meshing the domain and so the mesh presented on figure 2.7 was created. This figure represents the computational domain of the BEM described in section 2.5.1. The nacelle of the turbine and the disk which models the blades are colored in gray. The boundary conditions are :

- uniform stream-wise velocity at the inlet ($1.13m \cdot s^{-1}$).
- uniform pressure at the outlet
- free-slip walls

The same array with a spacing of 7 rotor diameter has also been meshed.

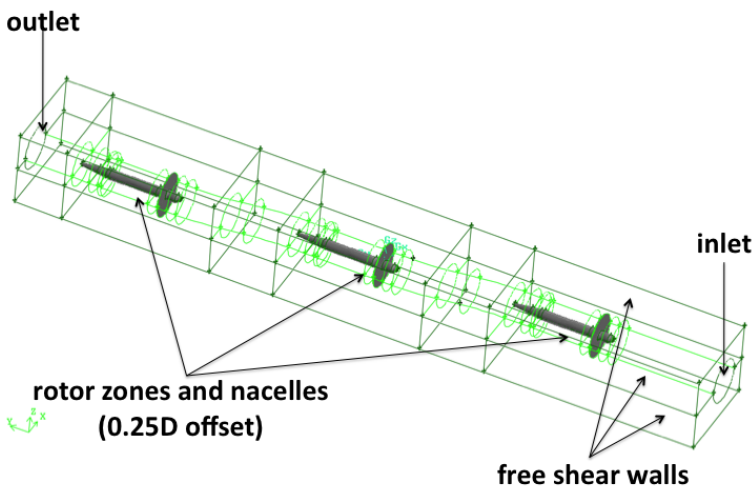

Figure 2.7: **Three turbines separated by 5 rotor diameters in the stream-wise direction and 0.25 rotor diameters in the transverse direction, meshed on GAMBIT.**

Even if the results are less sensitive than for SRF, the BEM model is an asset in terms of computational cost and turn-around time. Indeed, the use of a disk instead

of the blades greatly simplifies the mesh. A lot of time is saved during the meshing process and, as there is almost ten times less mesh elements than in the SRF mesh, the simulation is much faster. Moreover, the mesh is structured in the whole domain except in the two transition zones between the turbines, where there was no solution but create an unstructured mesh. But that was not a major concern since in the whole domain there is only 17 high-skewed elements (≈ 0.85) over almost one million elements.

Chapter 3

BEM SIMULATIONS OF AN ARRAY OF THREE TURBINES WITH 0.25D LATERAL OFFSET AND DOWNSTREAM SPACING OF 5D AND 7D

3.1 Simulation of Experimental Setup and Condition

In this section of the report, results of the performance and flow field simulation in arrays of three turbines with 0.25D lateral offset and downstream spacing of 5D and 7D are presented. The details about creating and meshing of the computational domains for these simulations were explained earlier in section 2.5.2. The ultimate goal of this study is to compare the numerical and experimental results against each other and highlight the level of application and limitation of the BEM for study of the performance and flow field in an array of MHK turbines. Therefore, the experimental setup and conditions developed previously [3] were matched in these simulations.

Before presentation of the simulations' results an important point about the challenge of matching the experimental operating conditions (i.e. turbine Tip Speed Ratio (TSR)) in the simulation should be explained. The TSR of a turbine is defined as:

$$TSR = \frac{r\omega}{V_{inc}}, \tag{3.1}$$

where r is the radius of turbine blade, ω is the rotor speed and V_{inc} is the incoming streamwise velocity into the rotor plane. TSR and Reynolds number are the two non-dimensional variables that set the efficiency of a MHK turbine. Within the experiment, a closed feedback control loop was used to control the angular velocity of the turbine and make sure the device is operating under the desired TSR [3]. On

the other hand, in numerical simulation there was no option to automatically control and adapt the downstream turbine's angular velocity as they operate in the wake of the upstream turbines. Thus, for the downstream turbines the TSR had to be set manually in the course of the simulations: a few hundred iterations were run, the incoming streamwise velocity 2D upstream of each turbines were averaged and the rotor speed for each device was set such that the experimental value of the TSR for that downstream turbine is matched in the simulation.

3.2 Results for a three-turbine array with 5D downstream spacing

Figure 3.1 shows the normalized velocity contours across the computational domain for an array of three turbines with 5D downstream spacing and 0.25D lateral offset. The velocity is normalized by the inlet velocity. In this simulation, the rotor speed of the three turbines were adjusted such that they all operated under the TSR=7.16.

As expected, the velocity in front of the upstream turbine is $1.13m \cdot s^{-1}$ (orange area). The wake of the first turbine is the area where the flow velocity is the lowest (green and yellow area). As the two downstream turbines are in this wake, it is expected that their efficiency will be lower than the one of the upstream turbine. It can also be noticed that the flow accelerates on the sides (red area). Indeed, the flow has to conserve mass flux. As the turbines blocks it near the centerline of the channel, the flow has to accelerate around the sides. That is why, in these areas, the flow velocity exceeds $1.13m \cdot s^{-1}$.

Figure 3.2 presents the comparison between experimental and numerical results for the array of three turbines with 0.25D lateral offset and 5D downstream spacing. This figure shows the efficiency of each turbine as a function of TSR.

The first interesting observation from these results is that the downstream-most turbine (red circles) is more efficient than the middle turbine (black circles) at all TSR values. At first sight, this seems illogical: the third turbine should receive less kinetic energy flux compared to the middle turbine, since it suffers the momentum

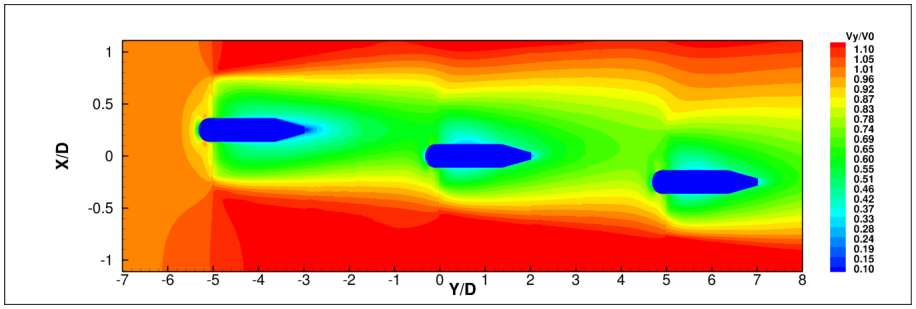

Figure 3.1: **Normalized streamwise velocity contours by the freestream velocity at the inlet for TSR=7.16**

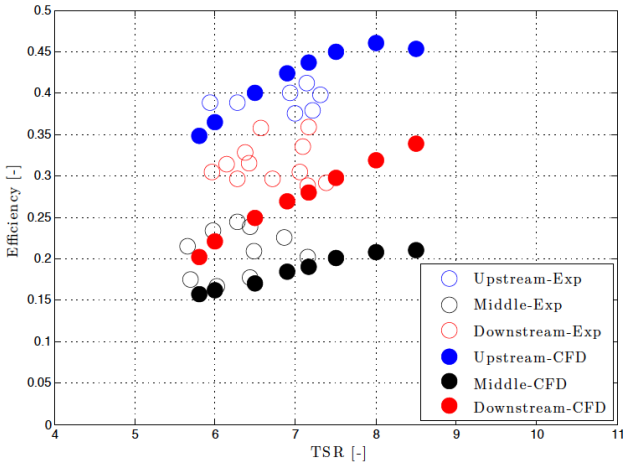

Figure 3.2: **Numerical versus experimental results for arrays of three turbines with 0.25D lateral offset 5D downstream spacing operating under various TSRs.**

deficit from both the upstream and the middle wakes, and therefore it should operate less efficiently at the same TSR. However, the numerical results show that the middle turbine increases the turbulent mixing process in the wake. This increment of turbulent mixing enhances the recovery of the wake, entraining high momentum fluid from the edges of the channel, and result in larger incoming kinetic energy flux into the

downstream turbine compared to the middle turbine.

Figure 3.3 confirms the above explanation. The top part of figure 3.3 visualizes contours of the normalized kinetic energy flux 2D upstream of each turbine. As these numerical results show, the incoming kinetic energy flux of the downstream turbine increases by about 25%. Furthermore, the bottom part of the figure 3.3 shows the averaged turbulent kinetic energy 2D upstream of the downstream turbine increases by about 40% compared to the middle turbine. Therefore, it can be concluded that the enhancement of the turbulent mixing process due to the middle turbine, enhances the efficiency of the downstream turbine at all TSR values.

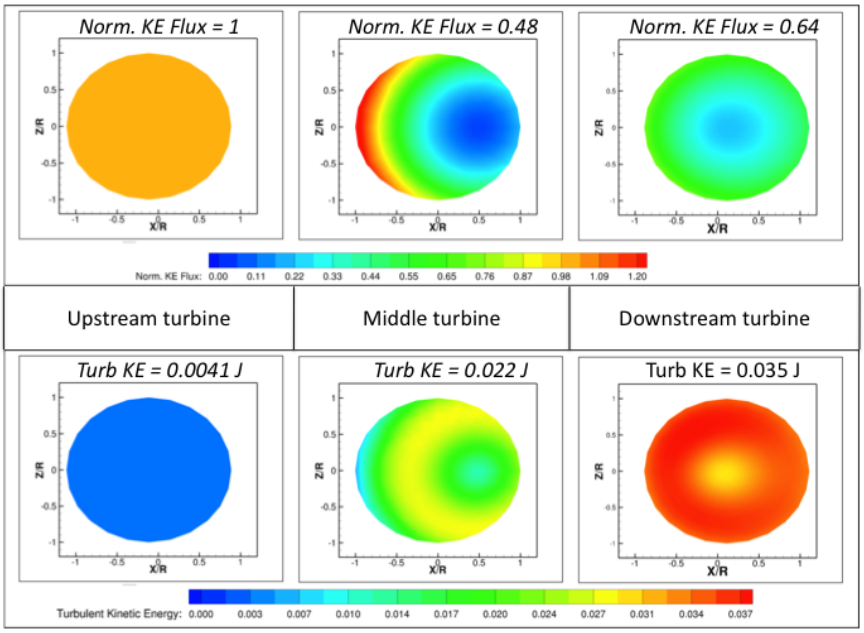

Figure 3.3: **Normalized kinetic energy flux and Turbulent kinetic energy in front of each turbine for a TSR=8**

Now, we will focus on comparisons between the three turbines efficiency curves from the experimental and numerical investigations. To perform this comparison, the curves showed in figure 3.2 are divided into three separate sections as follows:

- Region of low TSRs (<7)
- Region of optimum TSR ($\sim$ 7 to 8)
- Region of high TSRs (> 8)

Region of low TSRs (<7) For lower TSR, it can be noticed that the agreement between experiment and numerical data has a large relative error ($\approx 30\%$). Indeed, the efficiency predicted with numerical model is lower than the one given by experiment. For experiments, when the TSR is decreased, the efficiency does not decrease as expected. Indeed, decreasing the TSR increases the AOA, and increasing the AOA should bring the flow separation closer to the blade tip and thus decrease the efficiency. According to T. Javerherchi's work [4] and N. Stelzenmuller's MSc Thesis [3], this counter-intuitive result seems to be due to a phenomenon that CFD does not accurately reproduce: the fluctuation of the blade rotor speed induces changes in the separation behaviour, a phenomenon sometimes referred to as "dynamic stall". Indeed, experiments show that at low TSRs, the fluctuations of the blade angular velocity increase significantly. This would affect the flow separation on the blade and therefore the efficiency.

Figure 3.4, taken from N. Stelzenmuller MSc thesis [3], shows the temporal variation of the rotor speed of one turbine operating at two TSRs (5 and 10). It confirms that the rotational velocity fluctuates significantly at lower TSR, whereas it does with a small amplitude at higher TSR. Therefore, the difference between numerical and experimental results lie in the fact that numerical models predict the theoretical efficiency curve, where the efficiency decreases with TSR, because the rotor speed of the blade does not fluctuate in CFD. It is important to notice that, for full-scale turbines, these fluctuations are unwanted due to fatigue considerations, and would be suppressed in a real-life prototype. So, even for low TSR, numerical results are representative of the expected performance of full-scale prototypes.

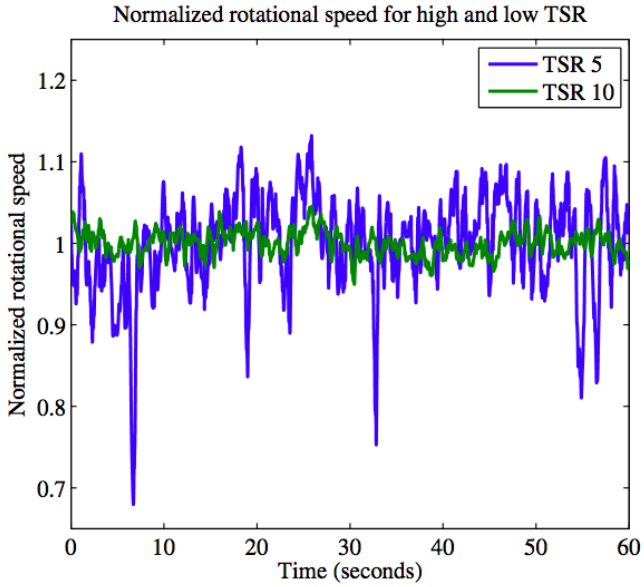

Figure 3.4: **Rotational speed normalized by mean rotational speed over one minute for a high TSR operating condition and a low TSR operating condition.**

Region the optimum TSR. For $7 < TSR < 8$, figure 3.2 shows a good agreement between experimental and numerical results. Only one aspect needs to be explained: for CFD, the optimum TSR is not the same than the experimental one. Indeed, as shown in N. Stelzenmuller's thesis [3], for experiments the peak of efficiency is reached around $TSR = 7$. But, on figure 3.2, one can see that the first turbine is predicted by the computations to reach a peak at $TSR = 8$. This value is closer to the theoretical value because, as explained above, the phenomenon of rpm fluctuations in experiments shifts the peak of efficiency to lower TSR. The reason for the discrepancy is that, in the numerical simulations, when the TSR is decreased from 8, the AOA increases and so the flow begins separating from the blade. That causes a loss of efficiency. Whereas, in experiment, even if the AOA increases, the fluctuation of the angular velocity delays the separation of the flow. Thus, even if the TSR is decreased

from its optimal value, the efficiency keeps growing.

Region of high TSRs. For higher TSR, despite the lack of experimental data, the numerical results are not expected. On figure 3.2, the curves of the two downstream turbines do not show any peak. After $TSR = 8$, their efficiency does not decrease. We hypothesize that this is due to blockage effect.

Blockage effect has a direct effect on efficiency. There is no formula that accurately corrects for this effect, although many tests have been conducted over the last century, including pioneering work by Glauert [14]. So, in the next section, we will discuss the effect of blockage on the performance of an array of turbines.

3.3 Differences between 5D and 7D spacing

All the numerical results for arrays of three turbines at 7D downstream spacing and 0.25D lateral offset are very similar to the results of arrays with 5D spacing. Figure 3.5 shows the numerical results for arrays with 5D spacing and 7D spacing. As expected, the two curves of the upstream turbine are overlaid. But for 7D spacing, the two downstream turbines are more efficient than for 5D. That is due to the fact that the flow has more space to recover, entrain high-momentum fluid from the channel edges, and to become more homogeneous. Therefore, the flow velocity in front of the downstream turbines is higher for 7D downstream spacing than for the 5D case.

3.4 Blockage effect

The blockage ratio (ϵ) is the ratio of the area of the circle swept by the blades and the cross-sectional area of the flume. This ratio defines the confinement of the flow. To see the effect of blockage on the array, two more meshes were created by doubling and quadrupling the cross-section of the flume. Therefore, three flumes were meshed with $\epsilon = 20\%$, $\epsilon = 10\%$ and $\epsilon = 5\%$. Efficiency as a function of TSR, for these three flumes, is given in figure 3.6. It gives several information about the effect of blockage

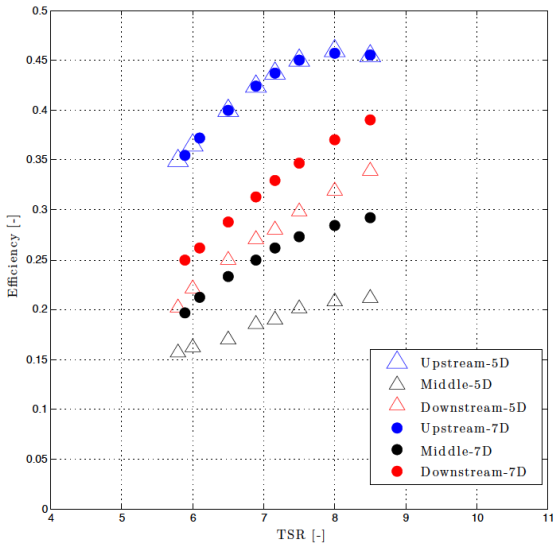

Figure 3.5: **Numerical results for arrays of three 0.25D lateral offset turbines with 7D downstream spacing, versus 5D spacing, at different TSR.**

on efficiency.

Blockage creates a gain of efficiency. The first remarkable observation from figure 3.6 is that increasing the blockage causes a gain of efficiency. Indeed, increasing the confinement means increasing the incoming flow velocity through each turbine rotor disk. That means increasing the available kinetic energy and therefore the efficiency of each turbine.

Blockage shifts the peak of efficiency. Each blade profile is designed to operate under an optimum TSR in an infinite flume. This optimum TSR for the turbines studied in this work is 7.5. But, as shown on figure 3.6, in the most confined flume (with $\epsilon = 20\%$), $TSR_{opt} = 8$ for the upstream turbine. Figure 3.6 also shows that decreasing ϵ shifts the optimal TSR toward 7.5 (the optimal value for $\epsilon = 0$).

To explain this fact, an important point is to define the AOA (α) :

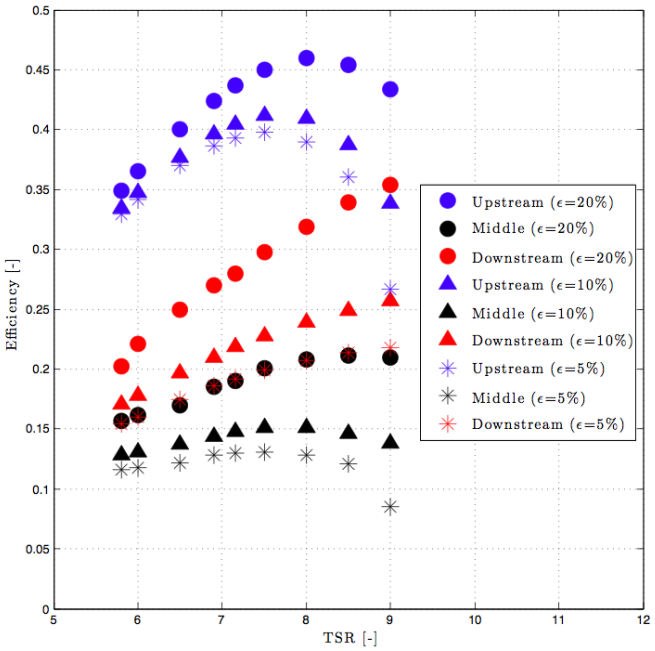

Figure 3.6: **Numerical results for arrays of three turbines at 0.25D lateral offset and 5D downstream spacing, simulated at various blockage ratios.**

$$\alpha(r) = \arctan \frac{V_{inc}(r)}{r\omega} + \beta(r) \tag{3.2}$$

where $\beta(r)$ is the twist angle depending of the position along the blade. We said that each turbine is designed to operate under an optimal TSR. To do that, the manufacturer adjusts this angle along the blade. So it is fixed and cannot be changed.

On figure 3.6, the shift of efficiency is hard to explain because the blockage has an effect on several variables. That is why figure 3.7 was created with three curves :

- The blue one : $\epsilon = 5\%$
- The red one : $\epsilon = 20\%$
- The black one : this curve has no physical meaning. It would be the curve for

ϵ = 20% if blockage had only an effect on the kinetic energy flux across the rotor disk. Indeed, the efficiency curve would be the same shape than at 5% blockage but higher.

That is why, now, we will focus only on the black and red curves to explain qualitatively why blockage shifts the peak of efficiency.

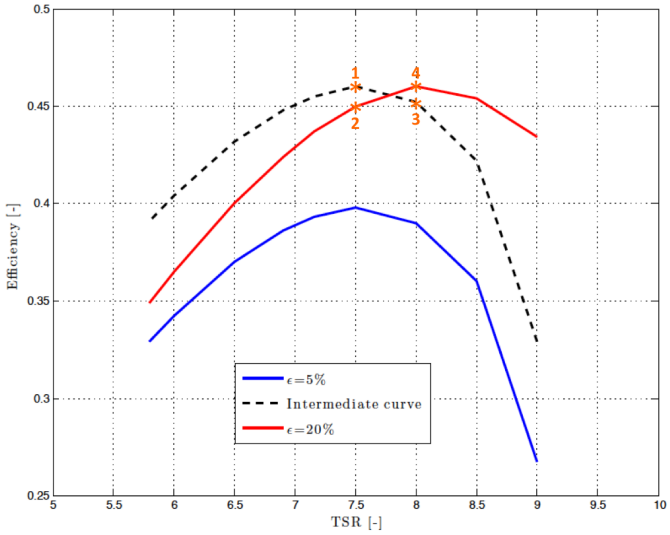

Figure 3.7: **Qualitative explanation of the shift of efficiency due to blockage for a single turbine operating under various TSR.**

For a better understanding, figure 3.8 shows the lift coefficient as a function the AOA for a NACA4415 profile. Points #1 to #4 correspond to the ones of figure 3.7. They have been placed qualitatively.

- At point #1 of η-TSR curve (figure 3.7), $\eta = \eta_{max}$, the corresponding lift coefficient is C_{Lmax} thus $AOA = AOA_{opt}$. Then, the TSR is kept constant but the blockage is increased. This causes the increase of V_{inc} and, therefore, the increase of the AOA, with $AOA > AOA_{opt}$. Thus, C_L decreases because the

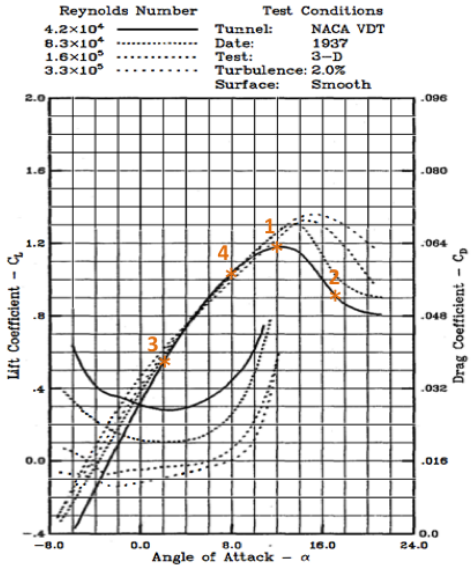

Figure 3.8: **Lift coefficient as a function of Angle of Attack for a NACA4415 profile (Points are placed qualitatively).**

flow separates from the blade, and as a consequence, the efficiency decreases. That explains the position of point #2 on figure 3.7. Therefore, in this case, increasing blockage means decreasing efficiency.

- Now, at point #3 on η-TSR curve, the TSR is higher than the TSR of point #1. As a consequence, $AOA < AOA_{opt}$, thus $C_L < C_{Lmax}$. Then, as previously, the TSR is kept constant but the confinement is increased. That induces the increase of V_{inc} and, so, the increase of the AOA. Therefore, C_L increases and η increase. That explains the position of point #4 on figure 3.7. In that case, increasing blockage means increasing efficiency.

Thus, increasing blockage will shift the peak of efficiency from its theoretical position to a position at higher TSR.

The Compound Effect of Blockage, Wake and Shear Flow on the Efficiency of the two Downstream turbines. As discussed in the previous section, increases in the blockage ratio result in a shift of the optimum TSR of the turbines in an array toward higher values. This shift of the optimum TSR is clear for the most-upstream and middle devices. As shown in figure 3.6 for the most-upstream and middle turbine, blue and black curves respectively, as the blockage ratio increases the optimum TSR for the curves corresponding to 20% blockage ratio shift toward higher values.

An interesting point in the results shown in figure 3.6 is the effect of blockage on the performance curve of the downstream-most turbine (red curve). For this device, with the increase in the blockage ratio from 5% to 20% the efficiency of the turbine continues to monotonically increase as the TSR value increases. Therefore, the shift of the optimum TSR is not clearly observed on this curve. The hypothesis behind this observation is that for the downstream-most turbine, the turbulent wake of the two upstream turbines and the shear flow due to the offset between devices are added effects to the blockage ratio, and exarcebate the effect of the blockage. In order to quantify the effect of each of these variables, turbulent wake and shear flow in the wake, they should be isolated and undergo further in depth investigation.

Chapter 4

THE SRF STUDY

4.1 MHK Turbine Array Simulations using Single Reference Frame (SRF) Model

The purpose of this study is to develop a general numerical methodology for characterization of the performance and flow field in arrays of horizontal axis MHK turbines using Single Reference Frame (SRF) model. To increase the level of confidence and validity of this numerical methodology, the previously developed experimental setup and results [3] are matched and simulated using the above-mentioned numerical methodology. As explained earlier in 2.2 in these simulations the Reynolds Averaged Navier-Stokes equations (2.6) integrated with an appropriate turbulent closure model are solved using the SRF model 2.3 in a commercial Computational Fluid Dynamics (CFD) package (ANSYS FLUENT). The predicted turbine's integral variables (i.e torque and efficiency) and the modeled wake are compared against the corresponding measured variables in the experiment.

4.1.1 Efficiency Formulation in SRF Model

In the SRF model's computational domain the blade span is discretized into small sections from the root to the tip. In the simulation the net hydrodynamic forces on each blade section resulted into a local torque on each blade section around the device axis of rotation. The net force and position for the center of pressure at each section and therefore the resultant local torque is calculated along the blade span as follows:

$$T_i = F_i * z_i. \tag{4.1}$$

In this equation z_i is the position of the center of pressure and F_i is the net perpendicular hydrodynamic force on each blade section that creates the local torque, T_i. The total torque and power created along the blade span is defined as:

$$T = \sum_i T_i. \tag{4.2}$$

The expression of the total power extracted from the flow by the entire turbine (with two blades) is:

$$P = 2 * T * \omega, \tag{4.3}$$

where T is the total torque and ω is the turbine's angular velocity. The efficiency of the turbine relative to available kinetic energy flux in the undisturbed flow at the inlet is defined as:

$$\eta = \frac{P_{extracted}}{P_{available}} = \frac{P}{\frac{1}{2}\rho A U_\infty^3}. \tag{4.4}$$

Where A is the area of the rotor and U_∞ is the incoming velocity.

Chronological Steps of the Investigation

At the first phase of the SRF simulations the SST k-ω turbulence model is used to close and solve the RANS equations. This choice of the closure model was recommended by T.Javaherchi et al. for simulation of a single MHK turbine using the SRF model. They showed that the SST k-ω turbulence model is capable of predicting the performance and wake of a single turbine with acceptable level of accuracy compared to the experimental results [4][13]. It should be noted that the required computational time for this simulation, initialized by the inlet boundary conditions and being run on a local server with fourteen 64 bit AMD CUPs, is about four days until a satisfactory converge could be obtained.

Table 4.1 shows the comparison between the predicted and measured efficiency of the two turbines at Tip Speed Ratio of 7.16. As shown in table 4.1 the predicted efficiency of the first turbine (0.4) is in a good agreement with the corresponding measured value in experiment. However the predicted efficiency for the second turbine (0.05) is significantly underestimated in this simulation. The hypothesis for this inaccuracy is that the observed overestimation of the velocity deficit in the wake of the first turbine, the incoming velocity of the second blade, is mainly responsible for this disagreement between the numerical and experimental value of efficiency for the second turbine. Figure 4.1 shows the comparison between the measured and predicted velocity deficits at two stations, 2 and 3 diameters downstream the first turbine. As shown in this figure the velocity deficit modeled with the SRF is overestimated. Therefore, in the next phase of this study the accuracy, capabilities and limitation of the turbulence model in simulating the wake of the turbines are investigated in more depth.

	Experiment	**SST** k-ω	k-ϵ
Turbine 1	0.40	0.405	0.257
Turbine 2	0.15	0.051	0.034

Table 4.1: **Comparison between the measured and predicted turbine efficiency in an array of two coaxial turbines with 5D fixed spacing.**

In the next phase of the investigation, simulation is run with the k-ϵ closure model. As discussed earlier in section 2.3, k-ϵ model is known to be a better choice to simulate the far wake region of an obstacle in a flow. The goal of this change in turbulence model is to investigate how much the efficiency of the first and second turbine will be affected and whether or not the change in the simulated wake structure of the first device would improve the efficiency of the second device.

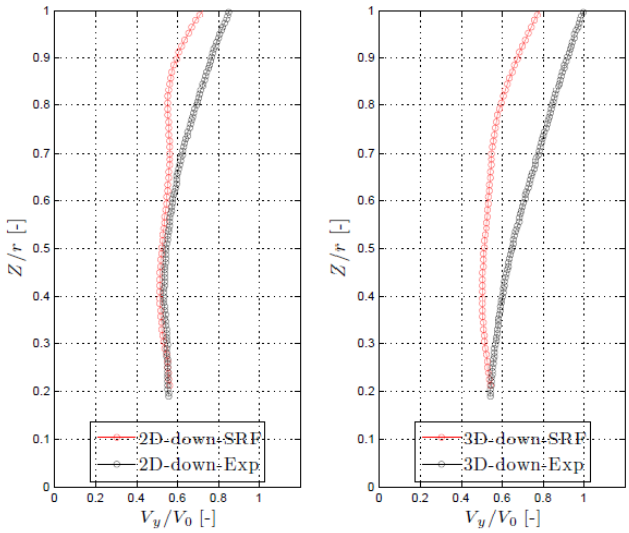

Figure 4.1: **Comparison of measured and predicted variation of the velocity deficit at various distances downstream of the first turbine, with TSR=7.16.**

As shown in table 4.1 the predicted efficiency for neither turbines using k-ϵ closure model are in agreement with the experimental results. The reason behind this differences is hypothesized to be the previously discussed limitation of the k-ϵ closure model in capturing the turbulent boundary layer close to the wall regions. This limitation leads to decrement the first turbine's efficiency by about 35% and about 32% for the efficiency of the second turbine compared to the results from the SST k-ω closure model. Since the predicted efficiency values for both turbine by the k-ϵ closure model are too far from the experimental one, it is decided to focus back on the SST k-ω model, in which at least the efficiency of the first turbine was predicted accurately. At this stage the investigation can be focused on the reason why the wake structure and therefore the velocity deficit of the first turbine is overestimated with the SST k-ω. Finding the answer to this question could provide insight to overcome this issue

and therefore improve the value of the predicted efficiency of the second turbine.

4.2 Investigation on the Issue of the SST k-ω Model in Modeling the Far Wake Region

4.2.1 Location of the problem

When the results of the SST k-ω model are compared against experiment, it appears that the efficiency of the first turbines are almost the same, but the second turbine is three times less efficient on the numerical simulation. The velocity deficit on the wake of the first turbine, which was already overestimated on previous works [4], is the first explanation of this lack of efficiency. It is obvious, according to Figure4.1 that the velocity on the simulation is under-estimated compared to the experiment. The reason behind this velocity deficit is hypothesized to be the characterization of the first turbine wake.

In order to confirm this hypothesis, a simulation is run on the VBM model, with the same conditions. The angular velocity of the two turbines are set as $\omega_1 = \omega 2 = 36$ $rad.s^{-1}$, as it was in the experiment and in the SRF simulation.

	Efficiency
Turbine 1	0.39
Turbine 2	0.8

Table 4.2: **Results of the VBM experiment, SST k-ω model**

With this simulation, where almost the same results than the ones in the SRF simulation are obtained, confirming that the problem with the SST k-ω is located on the wake of the first turbine.

To solve this problem F. Menter, the creator of the SST k-ω model,was contacted through Fluent help. The conclusion of the discussion is the presence, in some equa-

tion of this model, of a factor which is reducing a lot the turbulence after the first blade, therefore the wake is recovering slowly and the velocity deficit on the wake is overestimated, then the efficiency of the second blade is lower than expected.

4.2.2 Investigation on the model equations

The equations which are giving the effective diffusivities for the SST k-ω model are the followings [17];

$$\Gamma_k = \mu + \frac{\mu_t}{\sigma_k} \tag{4.5}$$

$$\Gamma_\omega = \mu + \frac{\mu_t}{\sigma_\omega} \tag{4.6}$$

where σ_k and σ_ω are the turbulent numbers for k and ω,respectively. The turbulent viscosity is;

$$\mu_t = \frac{\rho k}{\omega} \frac{1}{\max(\frac{1}{\alpha^*}, \frac{SF_2}{a_1 \omega})} \tag{4.7}$$

where S is the strain rate magnitude, a_1=0.31 and is changeable, and $\alpha^* = 1$ for high-Reynolds number form of the k-ω model. The blending function F_2 is given by;

$$F_2 = \tanh(\phi_2^2) \tag{4.8}$$

$$\phi_2 = \max(2\frac{\sqrt{k}}{0.09\omega y}, \frac{500\mu}{\rho y^2 \omega}) \tag{4.9}$$

In our case, the minimum of the two terms of (4.9) is 50 on the entire domain. Therefore at least;

$$F_2 = \tanh(50^2) = 1 \tag{4.10}$$

As a consequence, for (4.7), its denominator shall be the maximum between 1 and $\frac{S}{a_1 \omega}$. If this value is greater than 1, then the turbulent viscosity is going to be clipped. It is assumed that this is the reason of the low efficiency on the second turbine. Therefore, if $\frac{S}{a_1 \omega} < 1$, the turbulent viscosity should not be clipped, and then the velocity on the wake of the first turbine should increase, and at the end, the efficiency of the second turbine should raise.

The only coefficient which is changeable is a_1. The maximum value of $\frac{S}{\omega}$ on the entire domain was 188.35. As a consequence, in order to have $\frac{S}{a_1\omega} < 1$, we must have $a_1 > 188.35$. With this value, it is certain that;

$$\Gamma_k = \mu + \mu_t \tag{4.11}$$

It has also been checked that this coefficient is used only on this equation, to not change anything else in the model. An important point is that this factor is one difference between the SST k-ω model and the standard k-ω model, therefore even by eliminating this factor, the modified SST k-ω model remains different from the standard k-ω model.

4.2.3 Results from simulations with the modified equations

After this investigation, the value of a_1 is modified in Fluent, and to have a safety margin, a_1 is set as $a_1 = 400$. A new simulation on the converged k-ϵ simulation is launched. Here are the results of this simulation;

	Experiment	**SST k-ω modified**
Turbine 1	0.40	0.302
Turbine 2	0.15	-0.062

Table 4.3: **Efficiency resuts of the first simulation with a_1 modified**

Obviously the turbulent limiter that should have been disabled is still in function. But it is assumed that something is incorrect on this simulation for the previous investigation was only based on mathematical definitions, with a physical interpretation of the variables defined. To confirm this investigation and the modification in the SST k-ω model, VBM simulation is run, to check the wake of the first turbine, for this model requires less computational time (two hours vs four days for the SRF).

This simulation with VBM matches the expectations, for the turbulent intensity on the wake of the first turbine is more important.

This in depth investigations shows that running the SRF simulation with new closure model from previously converged solution does not include the changes in model accurately. Therefore it is decided to re-run simulations with new closure models from scratch (i.e initialize the flow with inlet boundary conditions). Here (Fig4.2) are the results of the last simulation, compared to the first simulation with the standard SST k-ω model.

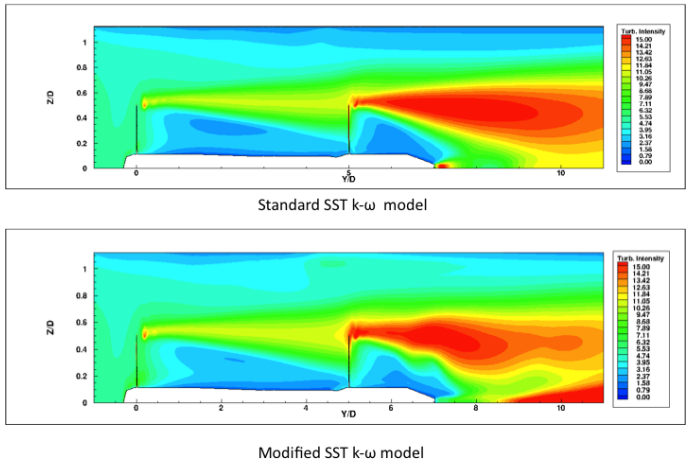

Figure 4.2: **Comparison of turbulent intensity between the standard SST k-ω model and the modified SST k-ω model.**

In the simulation with the modified SST k-ω model, the turbulent intensity in the wake of the first turbine is higher than with the standard model. This was the goal of the model modification. The followings assumptions were that benefiting from this turbulence, the wake would recover faster, therefore the velocity deficit would decrease, and the efficiency of the second turbine was expected to match the experimental data. The following figure (Fig4.3) is showing that the velocity deficit

remains overestimated even after the modification in the SST k-ω model.

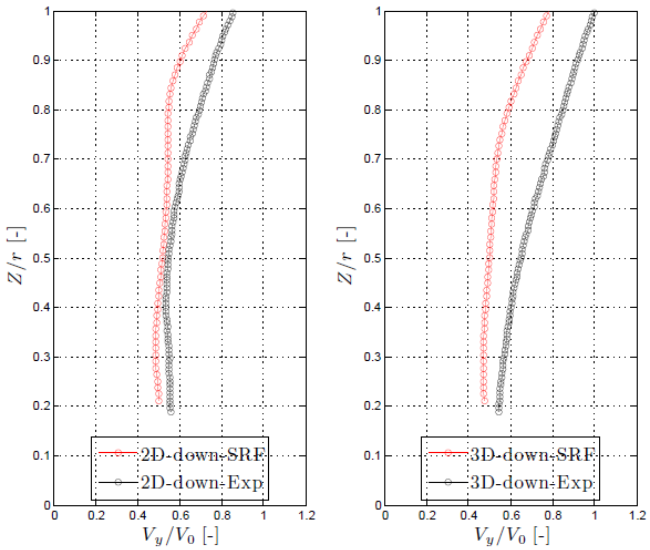

Figure 4.3: **Comparison of measured and predicted variation of the velocity deficit at various distances downstream of the first turbine, with TSR=7.16, using the modified SST k-ω model**

Therefore, due to the low velocity in front of the second turbine, its efficiency is no longer expecting to match the experimental data. In fact, as shown on Table4.4 the efficiency of both the two turbines are not matching the experiment, highlighting that something else is involved in the change which was made.

	Experiment	**SST k-ω modified and started from scratch**
Turbine 1	0.40	0.301
Turbine 2	0.15	-0.17

Table 4.4: **Efficiency resuts of the first simulation with a_1 modified**

The efficiency of the second turbine changed compared to the previous simulation

(Tab4.3), and the efficiency of the first turbine is almost the same. This demonstrates that the SRF simulation is very sensitive to modifications on the closure turbulence models. Whenever a modification in the choice of turbulence model is done on a simulation using SRF model, it should be started from scratch.
The trouble in these results is the negative efficiency of the second turbine. This means the second blade is acting as a propeller and no longer as a turbine.
Correlated to the low efficiency of the first turbine, this highlights that the change which was executed in the SST k-ω model acted as predicted for the turbulence intensity but had also other consequences, not expected.

4.2.4 Summary and Conclusions

In summary our investigations showed that the currently used turbulence closure models (i.e. SST k-ω and k-ϵ) performed poorly in simulation of the flow field in the wake of the turbines where turbulent intensity is very high (5-10 %). Since the SST k-ω model leads into a good agreement between numerical and experimental results for the performance of the first turbine and its near wake region, 2D downstream, it was decided to focus back on the reason behind the limitation of SST k-ω in modeling the far wake region of the flow.

Our investigations revealed that the implemented turbulent viscosity limiter in the SST k-ω closure model is the strongest suspect in underestimating the turbulence in the far wake and therefore underestimating the velocity deficit recovery process compared to the experimental results. After that the value of the a_1 constant was changed, it was observed that the turbulent intensity in the wakes of both turbines increased. However, this increment did not show a significant affect on the mean flow and the velocity deficit profiles in the wake. Our hypothesis is that the modification of the constant a_1 inside the SST k-ω closure model affected the main sources of the turbulent wakes, which is the turbulent boundary layer around the blade span of tur-

bines one and two, significantly and this led to change of the wake structure of both turbines. This can be confirmed by looking at the decrease in the efficiency values of both turbines predicted with the modified SST k-ω model.

In conclusion it is recommended to investigate on other possible approaches to modify the SST k-ω model so that its limitation for simulation of the far wake is improved. It should be noted that this modification has to be done without effecting the flow field simulations around the blade span. An alternative recommendation is to test other available turbulence closure models implemented in the CFD commercial package to perform flow field simulations in this type of turbine array with tight spacing and high turbulent intensity.

Chapter 5

CONCLUSIONS AND FUTURE WORK

5.1 Array of three turbines

For arrays of three turbines with a lateraloffset, good agreement between numerical and experimental results was achieved. Where there were significant discrepancies, we were able to explain the physical mechanism behind those. Therefore, the results are exploitable and some conclusions can be drawn:

- The downstream turbine is more efficient than the middle one. The reason is that the middle turbine mixes the flow, so the third one receives more kinetic energy than the second one. Therefore, one solution to be explored should be to use a grid to generate a mixing of the flow instead of the middle turbine.

- Blockage has a strong effect on efficiency. Indeed, increasing the confinement increases the efficiency of the array of turbines. But, in that case, to operate under the optimum TSR, the turbines have to rotate faster therefore the structure may be exposed to higher stress. There are some advantages and some drawbacks in placing the turbines in a narrow channel. Future work will have to determine what is dominant among both the advantages and the drawbacks.

- When the downstream distance between the turbines is 7 rotor diameters, the two downstream turbines are more efficient than with a 5D spacing. Indeed, the wake has more space to recover. The tradeoff is that as the spacing between turbine rows is increased, fewer turbines can be placed in the array. Therefore, engineering/economic studies will have to be conducted to find the best distance between turbines.

5.2 Array of two coaxial turbines

For the array of two coaxial turbines, the results which have been obtained could not match the experiments. Despite this, significant progress has been made, especially in the understanding of the SST k-ω model. Some conclusions and proposal for future work can be made at the end of this study:

- The SRF model is highly sensitive to modifications of turbulence closure models. When the simulation is started with one turbulence mode, any change in closure models for this simulation will make the simulation converge to an inaccurate solution of the Reynolds-Averaged Navier-Stokes equations.

- The SST k-ω model is not accurate enough in modeling the wake of a turbine under high free-stream turbulence conditions. This has been noticed in the study of a single turbine and is confirmed in this report.

- A modification of the SST k-ω model can be conducted in order to increase the turbulence intensity on the field. This modification is not sufficient by itself to adapt this closure model to SRF turbines but is a first step on its improvement. Future work should extend this solution and investigate deeper on the model description.

- The mesh of this model was accurate enough to run simulations, but had to assume some simplifications, due to the limited time available for the meshing phase of this study. This mesh can be improved, and this enhancement may be the focus of future investigations.

BIBLIOGRAPHY

[1] Multiphase & cardiovascular flow lab. depts.washington.edu/fluid/lab, 2014.

[2] What is renewable energy? http://arena.gov.au/about-renewable-energy/, 2014.

[3] Stelzenmuller N. Marine hydrokinetic turbine array performance and wake characteristics. Master's thesis, University of Washington, 2013.

[4] Javaherchi T. *Numerical investigation of Marine Hydrokinetic Turbines: methodology development for single turbine and small array simulation, and application to flume and full-scale reference models.* PhD thesis, Washington State University, 2014.

[5] Deniset F. Hydrodynamique numérique, troisième partie: Mécanique des fluides numérique - notes de cours. Ecole Navale / VA GM, 2014.

[6] Kundu P. Cohen I. *Fluid mechanics, fourth edition.* Elsevier, 2008.

[7] Pope S. *Turbulent Flows.* Cambridge University Press, 2000.

[8] Javaherchi T. Numerical modeling of tidal turbines: Methodology development and potential physical environment effects. Master's thesis, University of Washington, 2010.

[9] Hirsch C. *Numerical computation of internal & external flows, second edition.* Elsevier, 2007.

[10] Javaherchi T. Antheaume S. Aliseda A. Hierarchical methodology for the numerical simulation of the flow field around and in the wake of horizontal axis

wind turbines: Rotating reference frame, blade element model and actuator disk model. *Wind Engineering*, 38(2), 2014.

[11] McLennan Andrew M. Turocy Theodore L. McKelvey, Richard D. *Gambit: Software Tools for Game Theory*, version 13.1.2 edition, 2014.

[12] Burton T. and Bossanyi E. Sharpe D., Jenjins N. *Wind energy handbook*. Wiley, 2000.

[13] Seydel J. Aliseda A. Javaherchi T., Stelzenmuller N. Experimental and numerical analysis of a scale-model horizontal axis hydrokinetic turbine. 2014.

[14] Polagye B. *Hydrodynamic Effects of Kinetic Power Extraction by In-Stream Tidal Turbines*. PhD thesis, University of Washington, 2009.

[15] Tomasini N. Tessier M. Numerical study of horizontal axis hydrokinetic turbines: Performance analysis and array optimization, 2012.

[16] Menter F. Improved two equation k-ϵ turbulence models for aerodynamic flows. *NASA Technical Memorandum*, (103975), October 1992.

[17] ANSYS Inc. *ANSYS Fluent 14.0 Theiry Guide*, April 2009.